LBNL Sustainable Systems SFA:
Evolution of Pore Structures and Flowpaths Challenge: Reactive Transport Modeling

Carl I. Steefel, Li Li, Li Yang, Mike Kowalsky, Kenneth Williams

Earth Sciences Division, Lawrence Berkeley National Laboratory

ABSTRACT

The major focus of research involved the assessment of the role of physical and chemical heterogeneities and pore clogging on the efficacy of uranium bioreduction. We examined the effects of physical and geochemical heterogeneities on the spatial distributions of mineral precipitates (principally calcite, FeS, elemental sulfur, and siderite) and biomass accumulated during a uranium bioremediation experiment near Rifle, Colorado. Field data were used to infer heterogeneous distributions of permeability and Fe(III) content through inverse transport modeling. After validating with field aqueous geochemical data, reactive transport modeling was used to estimate the spatial distribution of precipitates and biomass. The results show that the maximum mineral precipitation and biomass accumulation occurs in the vicinity of the injection wells and is dominated by sulfate reducing reaction products. Reduction of as much as 5.4% of the pore space is predicted to have occurred locally. Biomass accumulation near the injection wells is less affected by heterogeneity because both the electron donor (acetate) and acceptor (sulfate) are present in the aqueous phase. However, accumulation in the down-gradient regions is observed, and is dominated by the iron-reducing reaction products, with spatial distributions strongly controlled by both physical and geochemical heterogeneities.

A second research focus involves the modeling of column experiments for the purpose of elucidating the detailed reaction pathways associated with uranium bioreduction. We are developing thermodynamic/kinetic models for U(VI), V(V), and Fe(III) bioreduction following the pioneering approach of Jin and Bethke (2005) and Dale et al. (2006, 2008). The column experiments involved Rifle sediment and Rifle groundwater with a 5 mM acetate amendment. In agreement with the field experiments, uranium and vanadium removal was nearly quantitative. Sulfate reduction evidently began by at least 10 days, even though sulfide breakthrough did not occur until 45 days. At a midpoint between these times (28 days), an electron balance calculation indicates that virtually all of the acetate donor is accounted for by sulfate reduction, despite the fact that no sulfide is breaking through. This suggests a mechanism in which dissolved sulfide reduces Fe(III)-hydroxide abiotically. This pathway was confirmed by the identification of elemental sulfur at a concentration of 12.5 µmoles/g sediment, balancing the 25 µmoles/g hydroxylamine-extractable iron hydroxide.

APPROACH

Biostimulation is being used to promote the bioreduction of uranium at the Old Rifle site in Colorado. The bioremediation strategy leads to a complex reaction network involving both microbially-mediated and abiotic pathways (Fig. 1).

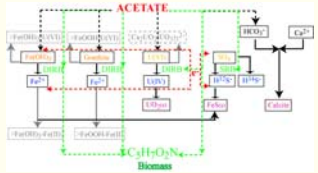

Figure 1: Reaction network for Rifle bioremediation.

The reactive transport code CrunchFlow was used to simulate the coupled transport, biogeochemical, and microbial processes for both the column and field experiments. Data from the column experiments were used to constrain the reaction network, establishing where possible both the pathways and rate constants.

Fe Reduction

$$FeOOH(s) + 1.925H^+ + 0.033NH_4^+ + 0.208CH_3COO^- \rightarrow Fe^{2+} + 0.033C_5H_7O_2N_{(s)} + 0.25HCO_3^- + 1.6H_2O$$

Uranium Reduction

$$UO_2^{2+} + 0.067NH_4^+ + 0.417CH_3COO^- + 0.8H_2O \rightarrow UO_2(s) + 0.0667C_5H_7O_2N + 0.5HCO_3^- + 2.15H^+$$

Sulfate Reduction

$$0.1155SO_4^{2-} + 0.125CH_3COO^- + 0.0057H^+ + 0.0038NH_4^+ \rightarrow 0.0038C_5H_7O_2N_{(SO_4)} + 0.114H_2O + 0.231HCO_3^- + 0.1155HS^-$$

Rate Laws

$$r_{FeR}^{Ac} = \mu_{FeR}^{Ac} B_{FeR} \frac{[FeOOH(s)]}{K_{S-FeR}^{FeOOH} + [FeOOH(s)]} \frac{[Ac]}{K_{S-FeR}^{Ac} + [Ac]} F_T$$

$$r_{FeR}^{Ac} = \mu_{FeR}^{Ac} B_{FeR} \frac{[UO_2^{2+}]}{K_{S-FeR}^{U} + [UO_2^{2+}]} \frac{[Ac]}{K_{S-FeR}^{Ac} + [Ac]} F_T$$

$$r_{SRB}^{Ac} = \mu_{SRB}^{Ac} B_{SRB} \frac{[SO_4^{2-}]}{K_{S-SRB}^{Ac} + [SO_4^{2-}]} \frac{[Ac]}{K_{S-SRB}^{Ac} + [Ac]} F_T$$

$$F_T = 1 - \exp\left(\frac{\Delta G_{NET}}{\chi_i^{Ed} RT}\right)$$

$$\Delta G_{NET} = \Delta G_r + m\Delta G_{ATP}$$

χ : Average stoichiometric number

ΔG_R Calculated from catabolic reaction only

Jin and Bethke, 2003, 2005

Abiotic reduction of Fe(III) by sulfide

$$2FeOOH + HS^- + 5H^+ \rightarrow 2Fe^{2+} + S_0 + 4H_2O$$

COLUMN EXPERIMENTS

With a 5 mM acetate injection, sulfate reduction in the column experiment began by at least 10 days, even though sulfide breakthrough did not occur until 45 days. At a midpoint between these times (28 days), an electron balance calculation (Fig. 2) indicates that virtually all of the acetate donor is accounted for by sulfate reduction, despite the fact that no sulfide is breaking through. This suggests a mechanism in which dissolved sulfide reduces Fe(III)-hydroxide abiotically. This pathway was confirmed by the identification of elemental sulfur (Fig. 3) at a concentration of 12.5 µmoles/g sediment, balancing the 25 µmoles/g hydroxylamine-extractable Fe-hydroxide.

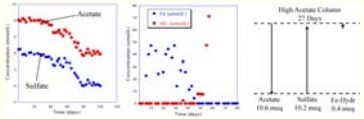

Figure 2: Electron balance at 28 days

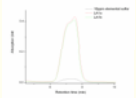

Figure 3: Chromatograph showing elemental sulfur extracted from column. The sulfur concentration was approximately 400 ppm. Elemental sulfur was analyzed by dissolving in acetone and analyzing with HPLC.

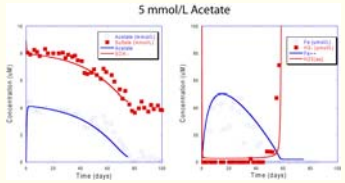

Figure 4: RT modeling of electron donors and acceptors. Breakthrough occurs where 25 µmole/g $Fe(OH)_3$ is consumed, indicating that 0.5 N hydroxylamine extraction targets both bioavailable and sulfide extractable Fe(III).

2D MODELING RESULTS

At the field scale, inversion of the tracer bromide breakthroughs in the same gallery in the 2002 and 2003 campaigns was carried out with the code ITOUGH, providing a high resolution 2D depth-averaged permeability field (Figure 3A). Selective extraction using 0.5 N hydroxylamine indicated an inverse correlation between grain size and Fe-hydroxide content, so a probability distribution for Fe(III) (Figure 3B) was constructed on a presumed inverse correlation with permeability.

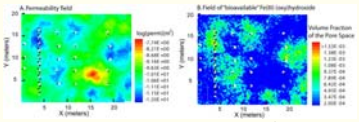

Figure 3: A) 2D depth-averaged permeability field based on inversion of bromide tracer data. Points refer to location of wells. B) Fe-hydroxide distribution based on probability model with inverse correlation between permeability and Fe(III).

Based on the permeability and Fe content fields shown in Figure 3, 2D reactive transport simulations were carried out. Figure 4 shows the match of the simulations to the acetate breakthrough data, while Figure 5 shows the 2D contour plots for bromide and acetate.

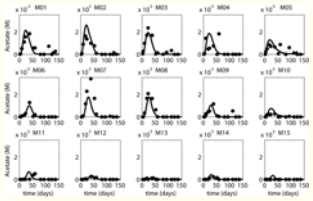

Figure 4: Comparison between acetate breakthrough data (dots) and RT simulations (lines) for 2002.

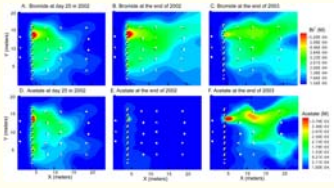

Figure 5: Contour plots for simulated bromide (top) and acetate during 2002 campaign.

Since a portion of the acetate goes to biomass growth, with the fraction dictated by the yield factor, the population of both Fe and sulfate reducers increase (Figure 6), although the patterns are different because the Fe reducers must follow the heterogeneous distribution of Fe-hydroxide in the sediment. There is no such requirement for the sulfate reducers, since both electron donors and acceptors are present in solution.

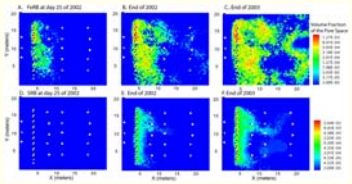

Figure 6: Spatial distributions of FeRB and SRB at day 25 in 2002, at the end of 2002, and at the end of 2003.

The precipitation leads to an accumulation of reaction products, especially calcite, magnesite, FeS, elemental sulfur, uraninite, and biomass, all of which reduce the porosity of the sediment (Fig. 7). The simulated total reduction in porosity is shown in Figure 8.

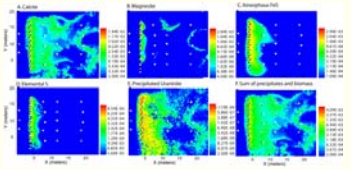

Figure 7: Simulation of spatial distributions of calcite, magnesite, FeS, elemental sulfur, uraninite, and biomass.

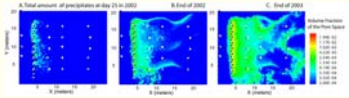

Figure 8: Total reduction in porosity from simulations.

SUMMARY

A combination of modeling and targeted chemical extractions and characterization have identified the importance of the reduction of Fe-hydroxide by dissolved sulfide via an abiotic pathway. In the case of one column experiment, this pathway accounts for nearly all of the Fe-hydroxide consumed. Moreover, both the mass of elemental sulfur and the breakthrough of dissolved sulfide from the column suggest that the 0.5 N hydroxylamine extraction method of Lovley and Phillips (1987) provides a good estimate of the bioavailable and sulfide-extractable Fe-hydroxide, although the important role of Fe(III) in clays is not discussed.

Two-dimensional RT simulations of the 2002 and 2003 biostimulation campaigns indicate that on a volume-averaged basis, porosity reduction as a result of mineral precipitation and biomass accumulation may be as high as 5.4%. Characterization of physical and chemical heterogeneity is essential in making these predictions quantitative.

ERSP ANNUAL PI MEETING APRIL 20-23, 2009

Funding for this study was provided by the U.S. Department of Energy, BER Program Contract DE-AC02-05-CH11231 for the Sustainable Systems Science Focus Area